Photophysics and Dynamics of Dye-Doped Conjugated Polymer Nanoparticles by Time-Resolved and Fluorescence Correlation Spectroscopy

ARTICLE *in* THE JOURNAL OF PHYSICAL CHEMISTRY C · DECEMBER 2013

Impact Factor: 4.77 · DOI: 10.1021/jp409570f

4 AUTHORS:

Santanu Bhattacharyya
Ludwig-Maximilians-University of Munich
26 PUBLICATIONS **195** CITATIONS
SEE PROFILE

Prashanthi Suthari
Indian Institute of Chemical Technology
14 PUBLICATIONS **115** CITATIONS
SEE PROFILE

Prakriti Bangal
Indian Institute of Chemical Technology
58 PUBLICATIONS **1,019** CITATIONS
SEE PROFILE

Amitava Patra
Indian Association for the Cultivation of Science
172 PUBLICATIONS **4,141** CITATIONS
SEE PROFILE

THE JOURNAL OF PHYSICAL CHEMISTRY C

Article

pubs.acs.org/JPCC

Photophysics and Dynamics of Dye-Doped Conjugated Polymer Nanoparticles by Time-Resolved and Fluorescence Correlation Spectroscopy

Santanu Bhattacharyya,[†] Suthari Prashanthi,[‡] Prakriti Ranjan Bangal,*[,‡] and Amitava Patra*[,†]

[†]Department of Materials Science, Indian Association for the Cultivation of Science, Kolkata 700 032, India

[‡]Inorganic and Physical Chemistry Division, CSIR-Indian Institute of Chemical Technology, Uppal Road, Tarnaka, Hyderabad 500607, India

Supporting Information

ABSTRACT: Fluorescent dye encapsulated conjugated polymer nanoparticles have been paid significant attention for potential applications in photonics and biophotonics due to their high brightness and better photostability. Bright, photostable, and monodispersed Nile Red (NR) dye encapsulated poly-*N*-vinylcarbazole (PVK) fluorescent polymer nanoparticles have been prepared to understand the influence of size of particles and the concentration of dye inside the particles on the photophysical properties by using steady-state, time-resolved fluorescence spectroscopy and fluorescence correlation spectroscopy (FCS). Here, we have quantitatively analyzed the hydrodynamic diameter, particle brightness, and population of NR molecules inside the particle with varying the particle size and NR concentration by using fluorescence correlation spectroscopy (FCS). The average fluorescence intensity of a single nanoparticle, i.e., per particle brightness (PPB) value, increases from 80 to 500 kHz, and the number of NR molecules per nanoparticle increases from 5 to 22 by increasing the concentration of NR from 0.5 to 1.8 wt % at the time of nanoparticle preparation. Fluorescence anisotropy study has been undertaken to understand the rotational dynamics of encapsulated NR molecules with varying particle size and NR concentration inside the nanoparticle. The particle brightness and quantum yield are enhanced due to increasing the radiative decay rate. Higher brightness (almost one order of magnitude higher with respect to free dye) and better photostability (15-fold enhancement) of these polymer nanoparticles are found to be efficient for bioimaging purposes.

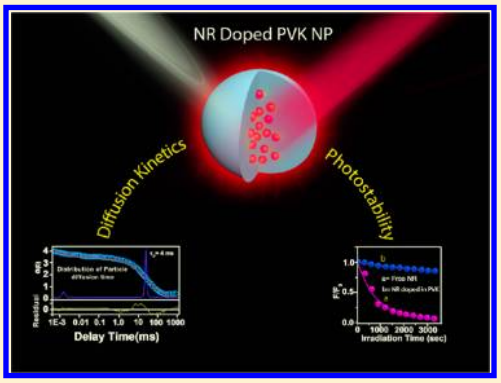

INTRODUCTION

Preparation of photostable, bright, and nontoxic fluorescent probes for biological applications remains a challenging subject in the nanoprobe research area.[1−13] Despite the recent advancements in the development of semiconductor and metal nanomaterials toward bioimaging, dye-encapsulated fluorescent polymer nanoparticles are a very promising fluorescent probe due to simple preparation, exceptionally bright and stable fluorescence, and the availability of biocompatible and functionally active polymer host materials.[14−23] Straightened out fundamental properties of the host polymers and guest dye molecules, size tunability of polymer particles, and protection of dye molecules against photo-oxidation and enzymatic degradation are a few advantages of such dye-encapsulated polymer nanoparticles. Recently, Chiu et al. highlighted the surface functionalization and biomolecular conjugation of polymer dots and their applications in biology and medicine.[23] They have also discussed the relationship between the physical properties and performance of polymer nanoparticles. Furthermore, emphasis has been given to electrospun nanofibers made of fluorescent polymer molecules.[24−26] Wang et al. have demonstrated the sensing capability of electrospun nanofibrous membranes of fluorescent polymer molecules.[24] Pisigano et al. have reported the laser emission properties of fluorescent dye encapsulated electrospun polymer nanofibers.[25] It is evident that significant attention has been given to fluorescent polymer nanomaterials to find out potential applications. However, there are some outstanding issues and uncertainties which need to be resolved for the better understanding of dye-encapsulated fluorescent polymer nanoparticles. These issues include local concentration of dye molecule, size distribution of nanoparticles, diffusion kinetics of nanoparticles, intracellular uptake of the nanoparticles, and relations among dye content, particle size, brightness, physiochemical stability, and biocompatibility.

Fluorescence correlation spectroscopy (FCS) is a powerful method for evaluating the fluorescence intensity fluctuations of fluorescent molecules or fluorescent nanoparticles in an extremely small (<fL) and well-defined confocal detection volume, which allows one to obtain fundamental properties of

Received: September 25, 2013
Revised: November 28, 2013
Published: December 2, 2013

fluorescent molecules or nanoparticles, such as diffusion coefficients, hydrodynamic radii, particle brightness, and concentration, in a single experiment.[10−13,27−34] Nienhaus and co-workers have demonstrated the protein adsorption onto colloidal nanoparticles by using fluorescence correlation spectroscopy.[35] Webb et al.[10] have quantified the number of dye molecules inside the silica nanoparticles and the quantum efficiency of the dye-doped silica nanoparticles using FCS study. In addition, the internal architecture of fluorescent silica particles has been elucidated by McDonagh et al. by using FCS study.[12] Larson et al.[10] have demonstrated the photophysical behaviors and diffusion phenomena of dye-doped silica NPs by changing the nanoparticle architecture and dimension. Recently, it was seen from FCS study that the colloidal properties of nanoparticles depend on surface chemistry, particle size, and interactions with different biomacromolecules.[27,30] Koynov et al. have used dual-color fluorescence cross-correlation spectroscopy (DC FCCS) to understand the coalescence and aggregation during nanoparticle preparation from emulsion.[28] Again, Ganguli et al. also studied the growth kinetics of nanorods in microemulsion using FCS study.[36] Quantitative fluorescence study of dye-encapsulated semiconducting polymer nanoparticles and their correlation with the undergoing photophysics of encapsulated dye molecules by changing nanoparticle size and population/distributions of the dopant dye molecules is very important for the development of unique nanoprobes for different photonics, opto-electronics, and imaging applications.

Our goal in this work is to engineer bright, photostable, and monodispersed Nile Red (NR) encapsulated poly-*N*-vinylcarbazole (PVK) benign fluorescent nanoparticles for potential applications. The influence of the size of particles and the concentration of NR inside the particles on the photophysical properties has been explored. FCS has been used to determine the hydrodynamic diameter and diffusion coefficient of NR encapsulated PVK nanoparticles and quantify the number of NR molecules inside the nanoparticles and brightness of the fluorescent nanoparticles. Interactions of the NR molecules, distributions of the NR molecules inside nanoparticles, and their population throughout the nanoparticles strongly influence the photophysical properties such as quantum yield and rotational dynamics of encapsulated NR molecules.[10,11] Steady-state and time-resolved spectroscopic studies are being used to understand the photophysical properties of NR encapsulated in polymer nanoparticles. Furthermore, the rotational motion of encapsulated NR molecules has been investigated using time-resolved anisotropy measurement with varying size of nanoparticles and concentration of NR. The modified photophysical properties and colloidal dynamics of NR-doped polymer nanoparticles could pave the way for designing a new fluorescent probe for bioimaging applications and to the development of theranostic tools and technologies.

EXPERIMENTAL SECTION

Materials. PVK [poly(9-vinylcarbazole)] (Aldrich), nile red (Sigma-Aldrich), distilled tetrahydrofuran (THF) (Aldrich), and deionized water (MERCK) were used as received for our synthesis in the present study.

Synthesis of PVK Nanoparticles. More than a month long stable PVK nanoparticles of different sizes with the same dye concentration and same size with different dye concentrations have been fabricated using our previously described method.[37] At first, NR was properly dissolved in dry THF making the concentration 4.2×10^{-5} M. On the other hand, in a separate vial PVK was properly dissolved in 10 mL of distilled THF overnight to make the concentration 1 mg/mL. After that, three different final stock THF solutions were prepared having a PVK concentration of 0.5, 0.3, and 0.15 mg/mL with fixed NR concentration of 1.5×10^{-5} M. Proper dilution was done by adding THF. The total volume of each of these three stock solutions was 2 mL. Finally, 500 μL of each of this stock solution was separately injected into 10 mL of deionized water under vigorous stirring conditions. Then, these three solutions were ultrasonicated for 15 min followed by partial vacuum evaporation of THF under 60 °C for 1.5 h. Therefore, we obtained three different sizes of NR-doped PVK polymer nanoparticles in aqueous suspensions. The optical density ratio of NR:PVK remains almost constant in stock THF and after nanoparticle formation in water. It confirms almost 100% yield of these dye-doped NPs. To ensure that all the dye molecules are encapsulated inside the polymeric nanoparticles we have used membrane dialysis having a molecular cutoff of 10−12 KD. In addition, we have also varied NR concentration inside the PVK polymer NP. To perform this, we have varied NR concentration of 0.6×10^{-5}, 1.5×10^{-5}, and 2.4×10^{-5} M separately in final stock THF solution where PVK concentration remains fixed (0.5 mg/mL). Then, a similar reprecipitation procedure has been done to ensure the formation of 0.5, 1.5, and 1.8 wt % NR-doped PVK NPs in 10 mL of aqueous solution.

Characterization. The morphological study of the NR-doped PVK nanoparticles was characterized by field emission scanning electron microscopy (FESEM, JEOL, JSM-6700F), and room-temperature optical absorption spectra were taken by a UV−vis spectrophotometer (Shimadzu). Room-temperature photoluminescence spectra were taken by a Fluoromax-P (Horiba JOBIN YVON) photoluminescence spectrophotometer. In TCSPC measurements, we used picosecond NANO-LED IBH-489 for 495 nm excitation of encapsulated NR molecules inside polymer nanoparticles. For anisotropy decays, we used a motorized polarizer in the emission side. The analyzer was rotated by 90° at regular intervals. The parallel ($I_{\parallel}$) and perpendicular ($I_{\perp}$) polarizations were collected alternatively until a certain peak difference between parallel and perpendicular decays was reached. The $r(t)$ value was calculated by the following formula[38]

$$r(t) = \frac{I_{\parallel}(t) - GI_{\perp}(t)}{I_{\parallel}(t) + 2GI_{\perp}(t)} \quad (1)$$

The analysis of the time-resolved data was done using IBH DAS, version 6 decay analysis software. The same software was used to analyze the anisotropy data. All experiments were done at room temperature.

FCS Measurements. The principles and confocal setup of the FCS have been well documented.[39−42] In this study, a home-built experimental setup was used and described elsewhere.[33] In brief, the 532 nm (PHOTOP, GDML-5020F) laser beam was focused into the sample through an objective lens (Olympus-60X, NA-1.20, water immersion). The fluorescence from the sample was collected by the same objective lens and refocused to the image plane by an achromatic lens (AC254-150-A1, THORLAB, USA) after separation from excitation laser light using a dichroic mirror (XF2016, 560DCLP, Omega-Optical-Inc., Vermont, USA). This signal was filtered by a band-pass filter (607AF75,

dx.doi.org/10.1021/jp409570f | J. Phys. Chem. C 2013, 117, 26750−26759

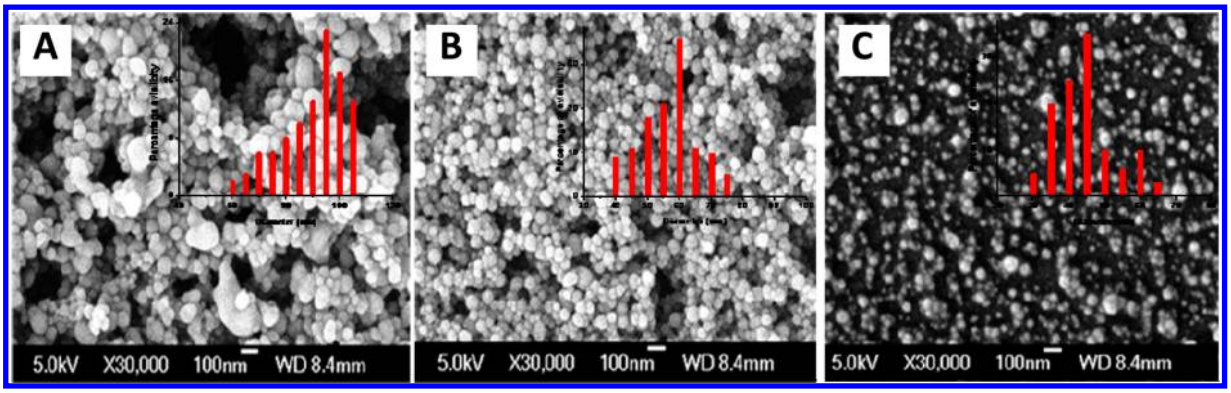

Figure 1. FESEM images of NR-doped PVK polymer NPs: (A) 100 nm, (B) 60 nm, and (C) 40 nm.

Omega-Optical-Inc., USA) to discriminate scattered laser light at the excitation wavelength and Raman scattered light of the solvent molecules if any. The isolated fluorescent signal was collected on a confocal point by a multimode fiber (radius 100 μm) and fed into an avalanche photodiode (APD) (SPCM-AQRH-13-FC, Perkin-Elmer Optoelectronic, Canada). The output signals of APD were processed by an autocorrelator (FLEX99OEM-12D, Correlator.com, USA) card, and correlated data were collected with home-built routine runs under LabVIEW. Using a neutral density filter (Thorlab), we kept the excitation laser power (at 532 nm) less than 5 mW to have excitation power at the sample volume 200−300 μW for all studies. All measurements were done at room temperature (25 ± 2) °C, and correlation curves were fitted with a single-component autocorrelation function to extract diffusion time.

In FCS, the observable is the fluctuation in fluorescence intensity measured within a focused laser volume (~fL). The normalized autocorrelation function (ACF) of temporal fluorescence fluctuations was carried out as in eq 2

$$G(\tau) = \frac{\langle \delta F(t)\delta F(t+\tau)\rangle}{\langle F(t)\rangle^2} \tag{2}$$

where $F(t)$ is the fluorescence intensity at time t, and τ is the time lag. δF is the fluctuation in fluorescence intensity relative to the average value $\langle F(t)\rangle$. For the case where translational diffusion of the molecules is the only process responsible for fluorescence fluctuations, the time-dependent part of the ACF for a single freely diffusing species in three-dimensional (3-D) Gaussian-shaped observation volume with radial (r) and axial length Z_Z is given by[33]

$$G_D(\tau) = \frac{1}{N}\left(1+\frac{\tau}{\tau_D}\right)^{-1}\left(1+\left(\frac{r_0}{Z_Z}\right)^2\frac{\tau}{\tau_D}\right)^{-1/2} \tag{3}$$

where N is the average number of molecules in observation volume. τ_D is the average residence time of the molecules in observation volume or lateral/translational diffusion time of the molecules across the observation volume. However, the most common dyes show a longer-lived triplet state (microsecond order), and during these intervals dye molecules cannot emit a fluorescence photon and appear as dark molecules. This triplet blinking appears as an additional shoulder in measured autocorrelation curves in short time scales. Since the formation of the triplet state is independent of diffusion dynamics, the overall ACF for a freely diffusing dye can be written by introducing the simplest additional term in ACF with characteristic triplet lifetime τ_T and amplitude A_T as follows[33]

$$G_D(\tau) = \frac{1}{N}\left(1+\frac{\tau}{\tau_D}\right)^{-1}\left(1+\left(\frac{r_0}{Z_Z}\right)^2\frac{\tau}{\tau_D}\right)^{-1/2} (1 + A_T e^{\tau/\tau_T}) \tag{4}$$

The diffusion constant (D) and hydrodynamic radius (R_h) of the molecules are then calculated according to

$$\tau_D = \frac{r_0}{4D} \tag{5}$$

$$D = \frac{kT}{6\pi\eta R_h} \tag{6}$$

where η is the solvent viscosity, k the Boltzmann constant, and T the temperature. Since the experimental setup influences the size of the observation (confocal) volume, we therefore perform autocorrelation studies with dilute (3 nM) aqueous solution RhB before the actual measurements and calibrate the r_0 value. For the present studies, the radial dimension of confocal volume of the system is 335 nm.

To obtain a better analysis of the size distribution of the nanoparticles, we have applied the maximum entropy method using 150 components, logarithmically spaced between 0.1 and 10 ms for the observed FCS data of the nanoparticles. This method is hereafter called MEMFCS, and it is developed by Profs. N. Periasamy and S. Maiti of TIFR, Mumbai, India.[33] Sengupta et al. showed that for heterogeneous systems a data-fitting algorithm for FCS based on the maximum entropy method (MEMFCS) yields much superior results in terms of distribution of different species over a conventional fit with a smaller number of components. The calibration part and sample preparation for FCS measurement for FCS are given in the Supporting Information.

RESULTS AND DISCUSSION

As-prepared NR-doped PVK nanoparticles with varying size and dye-to-polymer composition are characterized using field emission scanning electron microscopy (FESEM) and steady-state absorption and fluorescence spectroscopy. FESEM images as seen in Figure 1 confirm size-controlled preparation of ~40, ~60, and ~100 nm nanoparticles using 0.5, 0.25, and 0.50 mg/mL of PVK in tetrahydrofuran (THF). One of the challenges during the preparation of such nanoparticles is the aggregation of NR molecules and tailoring of the fundamental photophysical parameters of the dye. Notably, UV−vis absorption spectroscopic (Supporting Information Figure S1) studies rule out the aggregation behavior of dye molecules inside

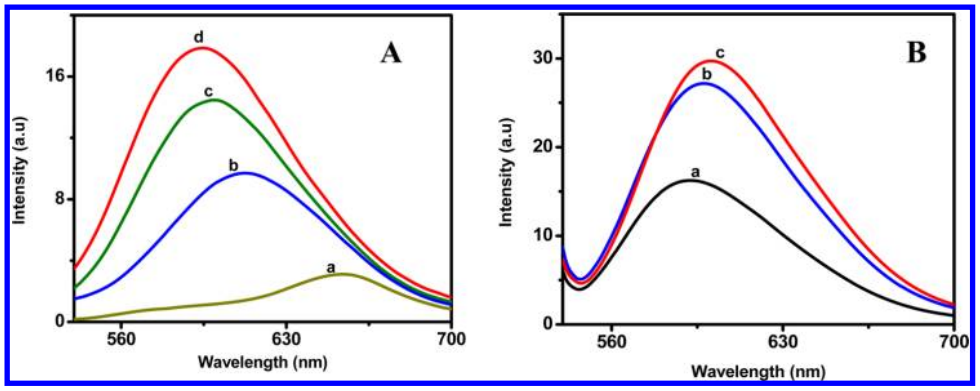

Figure 2. (A) Photoluminescence spectra of NR in water (a) and NR-doped 40 nm (b), 60 nm (c), and 100 nm (d) PVK polymer nanoparticles. (B) Photoluminescence spectra of 0.5 wt % (a), 1.5 wt % (b), and 1.8 wt % (c) NR dye doped PVK polymer nanoparticles.

nanoparticles at the studied concentrations. Only a hypsochromic shift of absorption maxima of encapsulated polymer nanoparticles suggests the solvatochromic nature of NR. The fluorescence (PL) spectra of free NR and 1.5 wt % NR doped in 40, 60, and 100 nm PVK polymer nanoparticles are recorded upon excitation at 530 nm (direct excitation of NR) (Figure 2A). The peak position of NR dye shifts toward higher energy, and the PL intensity increases after encapsulation of NR in the polymer matrix. A similar trend follows with increasing the particle size of the nanoparticle. This blue shifting of the PL spectra of NR molecules and increase of PL intensity on a gradual increase of the size of PVK nanoparticles indicates the gradual enrichment of hydrophobicity inside the nanoparticle matrix.[22] A larger number of PVK molecules effectively take part in single nanoparticle formation with increasing concentration. Therefore, intermolecular interactions as well as extent of aggregation increase with increasing the size of PVK polymer nanoparticles.[43] As a result, we observed red shifting in PL emission and excitation spectra with increasing the size of pure PVK nanoparticles (see Supporting Information Figure S2).[44,45] Thus, the hydrophobicity and rigidity are increased with increasing size of polymer nanoparticles which will influence NR molecules. As NR molecules are environmentally sensitive fluorophores and solvatochromic in nature, the hypsochromic shift of PL spectra is observed with increasing hydrophobicity. In addition, the PL spectra of NR inside the polymer nanoparticles are quite broad with respect to that of free NR, and it indicates nonhomogeneous behavior of NR inside the PVK nanoparticle matrix which is consistent with previous results.[46] Polymer nanoparticles are presumably formed due to coiling of the polymer chain.[20] Therefore, at the time of the chain coiling, there should be some confined/caged water molecules inside the polymer NP.[22] As a result, a certain fraction of encapsulated NR should reside with the direct contact of water and make H-bonding. On the other hand, the rest of the fraction resides in a more hydrophobic pocket due to direct contact with the hydrophobic polymer chain. This would be the reason behind heterogeneous distribution of NR inside the polymer nanoparticles. The quantum yield of free NR in water is calculated to be ~2%, whereas the quantum yields of NR-encapsulated nanoparticles increase with size of the particles. The values are found to be 7%, 16%, and 20% for 40, 60, and 100 nm PVK nanoparticle-encapsulated systems, respectively, while NR concentration is 1.5 wt %. Significant enhancement of quantum yield is due to encapsulation of dye. The low quantum yield of free NR in water indicates the faster nonradiative relaxation due to interaction with water.[10−12] On the other hand, the enhancement of quantum yield indicates the decrease of the nonradiative relaxation processes for encapsulated NR molecules inside the polymer matrix.[10] From the fundamental point of view, it is very important to estimate quantitatively the amount of dye diffusing from the nanoparticles (for different sizes) and the swelling of the nanoparticles in the solvent medium. To investigate these issues, we have taken the time-dependent PL emission of encapsulted NR dye molecules inside the different sizes of PVK polymer nanoparticles (see Supporting Information Figure S3). We have observed very little amount of PL quenching (3−5%) coming from NR dye molecules for all three sizes of polymer nanoparticles. We believe that such a kind of small diffusion rate of NR molecules does not effect the overall luminescence behavior of NR-doped PVK polymer nanoparticles for their further applications. Furthermore, the photoluminescence properties of encapsulated NR molecules with varying NR concentrations for a given fixed sized nanoparticle (such as 100 nm) have also been illustrated (Figure 2B). For the 0.5 wt % NR-encapsulated system, the emission maximum is at around 590 nm, and it is shifted toward the lower-energy side with increasing concentration of NR dye. The calculated quantum yields are 11%, 22%, and 24% for 0.5, 1.5, and 1.8 wt % NR-encapsulated systems, respectively. The difference in the fluorescence quantum yields is attributed to the surface to volume ratios of the nanoparticles; the smaller the particle size, the larger the number of NR molecules on the surface of nanoparticles.

Fluorescence Correlation Spectroscopy. Figure 3 shows fluorescence autocorrelation traces, individually collected for 60 s of the NR-doped PVK nanoparticles. This autocorrelation directly defines the unconstrained three-dimensional diffusion phenomena of three different sizes of PVK nanoparticles and measures their respective diffusion times (τ_D), residence time in optically defined focal volume. Conventional single-component fitting of autocorrelation data yields diffusion times of 4.1, 2.2, and 1.7 ms which correspond to the hydrodynamic radius ~56 ± 5, ~30 ± 3, and ~21 ± 2 nm of dye-doped PVK nanoparticles, respectively. These values nicely corroborated with the values obtained from FESEM analysis (depicted in Table 1). MEMFCS analysis shows a single distribution of diffusion time, and the distribution of particle sizes for these three different sized particles matches well with the peak position of the single-component fitting. This result is combined with the fact that particles are monodispersed in

dx.doi.org/10.1021/jp409570f | J. Phys. Chem. C 2013, 117, 26750−26759

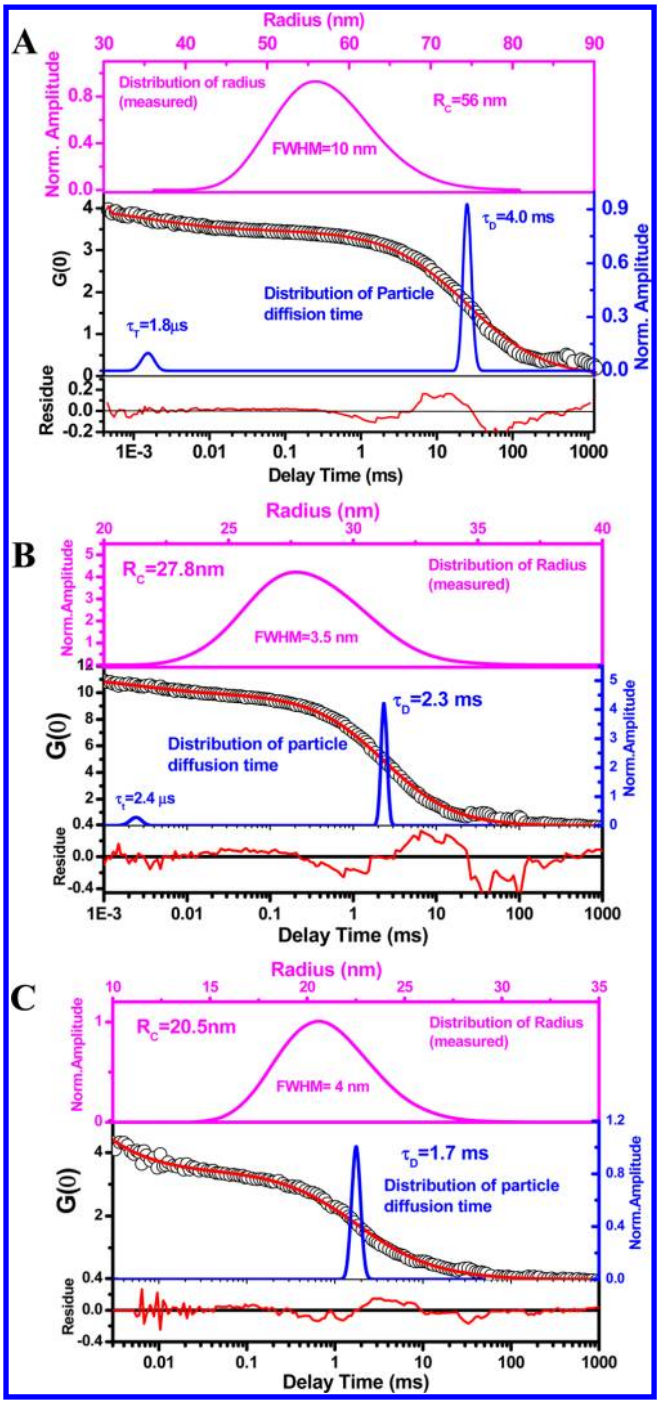

Figure 3. FCS data obtained by measuring NR-encapsulated PVK nanoparticles and resultant fittings. Upper panel of each figure shows the distribution of hydrodynamic radius; middle panel shows the autocorrelation curves (black circles), the resulting fitting of MEMFCS (red line), and the distribution profile of the diffusion time obtained by MEMFCS analysis (blue solid line); and the lower panel shows the residual plot of NR-doped (A) ∼100 nm, (B) ∼60 nm, and (C)∼40 nm PVK polymer nanoparticles.

nature. Particle size distributions are found to be exactly Gaussian with very narrow fwhm (∼4−10 nm), and the calculated diffusion coefficients of the particles are ∼1.11 × 10^{-11} to 6.42 × 10^{-12} m^2 s^{-1} for 40−100 nm of particle size, respectively. Thus, the hydrodynamic radius obtained from FCS paves the important utility of FCS for the determination of the exact size of this kind of polymeric colloidal nanoparticles

Table 1. Comparison of Sizes Obtained from FESEM and FCS Study

systems	average diameter obtained from FESEM (nm)	hydrodynamic diameter obtained from FCS study (nm)
NR-doped PVK 1	∼40	41 ± 4
NR-doped PVK 2	∼60	58 ± 6
NR-doped PVK 3	∼100	105 ± 10

which is consistent with other studies.[27,33] The calculated amplitude ($G(0)$) values of the autocorrelation indicate the number of diffusing particles in an optically defined focal volume which effectively provides the overall molar equivalent concentration of the observed nanoparticle colloids.[33,10] We have calculated the particle concentration of as-prepared aliquots which is of the order of ∼50−80 nM. Similarly, the average count rate is directly proportional to the photon collected from the same focal volume, and it helps to predict the intrinsic per particle brightness (PPB) of the diffusing particles.[10−12]

To assess the bioimaging potentials of the nanoparticles, we quantitatively evaluated the per particle brightness (PPB), which is average fluorescence intensity of a single nanoparticle, as a function of the particle size. It is measured from the average fluorescence intensity detected from the average number of nanoparticles in a defined excitation volume. Figure 4 illustrates both calculated PPB as functions of particle size and NR concentration. The calculated average PPBs are ∼250, ∼280, and ∼300 kHz for ∼40, ∼60, and ∼100 nm PVK polymer nanoparticles, respectively. The concentration of the NR plays an important role in PPB value, and the average PPB values are ∼80, 300, and 500 kHz for the 0.5, 1.5, and 1.8 wt % NR-doped system, respectively, when particle size is 100 nm which is almost exponentially dependent on the concentration of dye molecules. It is to be mentioned that poor fluorescence yield of free NR in aqueous solution does not provide traceable autocorrelation. Thus, we cannot compare PPB of the dye-doped PVK nanoparticle with free dye. Therefore, we use the PPB of Rhodamine B, which is 30 kHz for comparison. It is interesting to note that NR-doped PVK nanoparticles show brightness more than 1 order of magnitude higher than free Rhodamine B in aqueous solution, and it is comparable to the case of homogeneous dye-doped silica nanoparticle systems where PPB is reported to be 7−8 times brighter than free dye.[10] However, this observation for the present PVK nanoparticles reveals that the size of the nanoparticles and NR concentration strongly influences the brightness of particles. In this contrast, it is important to address how the number of NR molecules encapsulated per particle correlates with the enhancement of the observed particle brightness. The number of dye molecules per nanoparticle eventually affects the photophysics of encapsulated dye molecules inside polymer matrix. PPB analysis combined with optical density measurements help to presume the number of dye molecules per nanoparticle. The calculated dye molecules per particle are ∼5, ∼15, and ∼22, for 0.5, 1.5, and 1.8 wt % NR-doped PVK nanoparticles (size ∼100 nm), respectively. On the other hand, the number of dye molecules remains constant (1.5 wt % dye) for three different sizes of nanoparticles (depicted in Figure 4). A pictorial representation shows that although the number of dye molecules remains unaltered for three different size polymer nanoparticles, PPB

dx.doi.org/10.1021/jp409570f | J. Phys. Chem. C 2013, 117, 26750−26759

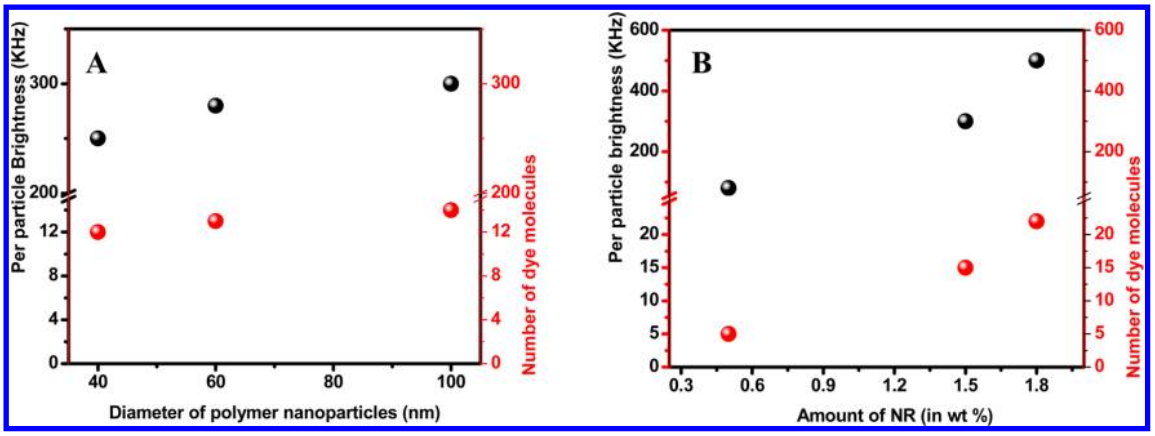

Figure 4. Particle brightness (black ball) and number of dye molecules per particle (red ball) with varying size of the polymer NP (A) and with varying the concentration of the dye inside the NP (B).

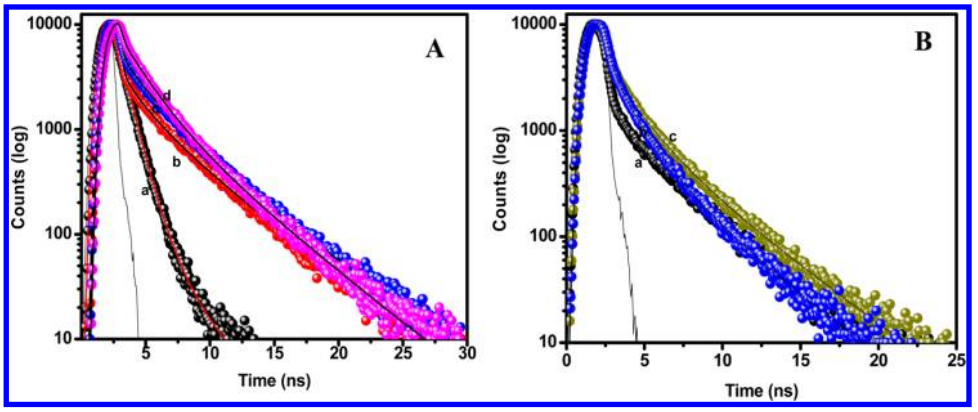

Figure 5. (A) Normalized time-resolved decay curves of pure NR in water (a), NR doped in 40 nm (b), 60 nm (c), and 100 nm (d) PVK polymer nanoparticles. (B) Normalized time-resolved decay curves of 0.5 wt % (a), 1.5 wt % (b), and 1.8 wt % (c) NR-doped PVK polymer nanoparticles.

values are increased linearly with varying size of the polymer nanoparticles. It may be due to the increased rigidity with increasing size of the polymer nanoparticles. In addition, for a particular size of polymer nanoparticles with varying NR concentration, the number of NR molecules per particle and per particle brightness increases almost in a similar fashion (exponentially). It may be due to the multiple NR incorporation, heterogeneous distributions, and excited state interactions of different conformations of dopant NR molecules. These are further unveiled by time-resolved spectroscopy later in this manuscript.

Time-Resolved Spectroscopy. Photophysical dynamics of NR dye molecules encapsulated in PVK nanoparticles as functions of particle size and the distribution of NR molecules within nanoparticles are important parameters that influence the fluorescence efficacy of the nanoparticles. Figure 5A shows the decay curves of free NR in water and encapsulated NR in 40, 60, and 100 nm PVK nanoparticles, respectively. For free NR, the decay curve fits well with the first-order kinetics. The lifetime of free NR is ~50 ps in water which is ascribed as the nonradiative twisted intramolecular charge transfer (TICT) state formation.[47] In accordance, the decay curves of NR encapsulated in different sizes of PVK polymer nanoparticles are fitted by biexponential decay kinetics. All these decay time values are listed in Table 2. The faster components are 90 ps (97%), 100 ps (86%), and 130 ps (75%) for 40, 60, and 100 nm PVK nanoparticles, respectively. On the other hand, the slower components are 1.77 ns (3%), 1.81 ns (14%), and 1.90 ns

Table 2. Fluoresence Decay Parameters of NR Dye and Dye-Encapsulated PVK Nanoparticles

systems	τ_1 (ps) a_1	τ_2 (ns) a_2	τ_{avg} (ns)
pure NR	50 (100%)	-----	
NR-doped 40 nm PVK NP	90 (97%)	1.77 (3%)	0.13
NR-doped 60 nm PVK NP	100 (86%)	1.81 (14%)	0.33
NR-doped 100 nm PVK NP	130 (75%)	1.90 (25%)	0.55

(25%) for 40, 60, and 100 nm PVK nanoparticles, respectively. The faster component of the decay kinetics confirms the formation of the TICT state of the dye molecule in available caged water inside the particle. It is known that the lifetime of the faster component increases with respect to that in bulk water.[48] It is already reported that the size of the PVK nanoparticles is tuned by increasing the amount of PVK molecules in precursor THF solution. Furthermore, more compact coiling is due to a greater extent of intermolecular interactions with increasing size of polymer nanoparticles. Therefore, NR molecules become gradually more confined with increasing size of the polymer nanoparticles.[22] On the other hand, the slower components designate the increase in hydrophobic interactions of NR molecules on increasing the size of the nanoparticles.[22] Further analysis shows that the amplitude of faster component of the decay profile increases with increasing dye population inside the nanoparticle of fixed size. It indicates a larger number of dye molecules are directly

dx.doi.org/10.1021/jp409570f | J. Phys. Chem. C 2013, 117, 26750−26759

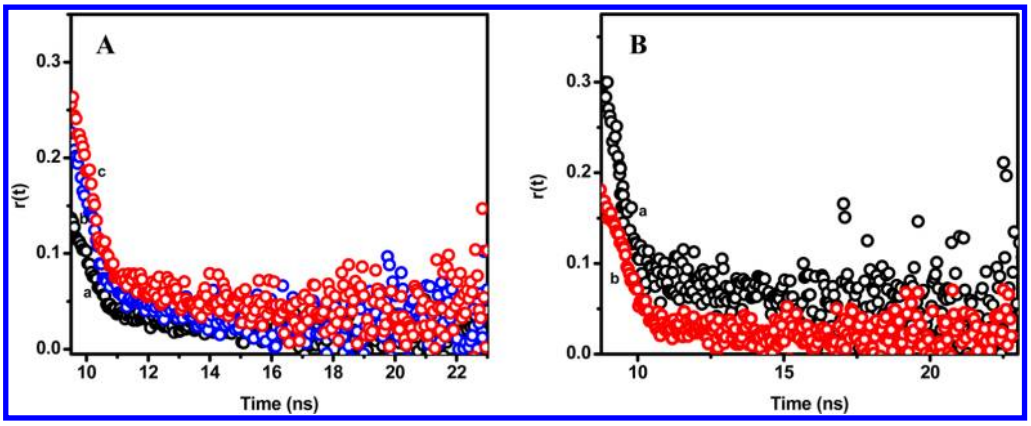

Figure 6. (A) Time-resolved anisotropy decay curves of NR-doped (a) 40 nm, (b) 60 nm, and (c) 100 nm PVK polymer nanoparticles. (B) Time-resolved anisotropy decay of (a) 0.5 wt % and (b) 1.8 wt % NR-doped PVK polymer nanoparticles.

interacting with the confined water molecules resulting in the greater extent of hydrogen bonding interactions with increasing dopant population at a fixed size of polymer nanoparticles. The calculated average lifetimes of NR are 0.28, 0.50, and 0.60 ns for 0.5, 1.5, and 1.8 wt % NR-doped ~100 nm PVK nanoparticles, respectively (Figure 5B). Due to the heterogeneous nature of the polymer matrix, NR molecules experience different local environments inside the nanoparticle depending on their overall population (polar environment and hydrophobic environment). The understanding of radiative and nonradiative decay rates due to encapsulation of NR molecules is one of the most fundamental issues for deeper insight into the photophysics of encapsulated NR molecules. The radiative and nonradiative decay rates are related to the quantum yield and the average decay time described elsewhere.[22] The radiative and nonradiative decay rates of free NR in water are 2×10^8 and 19.8×10^9 s^{-1}, respectively. However, in the case of encapsulated NR in PVK nanoparticles, the nonradiative decay rates are 5.9×10^9, 2.2×10^9, and 1.6×10^9 s^{-1}, and the radiative decay rates are 3.12×10^8, 3.5×10^8, and 4×10^8 s^{-1} for 40, 60, and 100 nm PVK nanoparticles, respectively. The large reduction of nonradiative decay rate and simultaneous enhancement of radiative decay rate are observed with increasing size of the PVK nanoparticles. The enhancement of radiative decay rate is due to hydrophobic encapsulation of the dye molecule inside the polymer matrix.[22] We have also calculated the radiative and nonradiative decay rate of NR with their different concentrations inside PVK polymer nanoparticles. In that case, radiative and nonradiative decay rates do not change noticeably. It may be due to the constant rigidity inside the polymer nanoparticles as the size of the polymer nanoparticles remains constant in this situation. Therefore, the brightness virtually depends on the population of dye molecules at constant size of the PVK nanoparticle.

Another important aspect of the encapsulation of dye molecules inside the polymer nanoparticles is their restricted motion which directly controls the photophysics of encapsulated NR molecules. To elucidate the relation between photophysics of encapsulated NR molecules and their rotational behaviors for the above-mentioned two different conditions (on varying size of PVK nanoparticles for fixed NR concentration and on varying concentration of NR inside the fixed size PVK nanoparticles), time-resolved fluorescence anisotropy measurement is performed. Before measuring the rotational behaviors of encapsulated dye molecule inside the nanoparticle, it is customary to measure the overall rotational motions of the nanoparticle itself because it can directly affect the rotational motions of the encapsulated NR molecules. To stop the overall rotation of the nanoparticles, we have measured the anisotropy decay in viscous medium (PEG). Interestingly, the decay profile remains almost similar with respect to normal aqueous suspension of the nanoparticles. It indicates that overall rotation of the nanoparticle does not affect the rotational motions of encapsulated dye molecules. As the size of the polymer nanoparticles is comparatively large, the rotational time of nanoparticles should effectively be in the microsecond region, and it cannot alter the comparatively faster rotational motions (in nanosecond scale) of the encapsulated NR molecules.[22,49] Figure 6A shows the time-resolved anisotropy curves of NR encapsulated in 40, 60, and 100 nm PVK polymer nanoparticles, respectively. All the fluorescence anisotropy decays are fitted with a biexponential function[38]

$$r(t) = r_0\left[a\exp\left(-\frac{t}{\tau_{slow}}\right) + (1-a)\exp\left(-\frac{t}{\tau_{fast}}\right)\right] \quad (7)$$

Here, τ_{slow} and τ_{fast} are the two reorientation times associated with the slow and fast motions of NR molecules in PVK polymer nanoparticles. 'a' is the pre-exponential factor which indicates the relative contributions of the slow and fast motions of the anisotropy decay. The average reorientation time $\langle\tau_r\rangle$ can be expressed as

$$\langle\tau_r\rangle = a\tau_{slow} + (1-a)\tau_{fast} \quad (8)$$

The observed $r(0)$ values are 0.14, 0.24, and 0.27 for 40, 60, and 100 nm PVK nanoparticle-encapsulated systems, respectively. The average reorientation times are 0.88, 1.86, and 2.01 ns for these three consecutive systems (40, 60, and 100 nm PVK). It is depicted in Table 3. It is obvious that the randomness of encapsulated NR molecules decreases on increasing the size of polymer nanoparticles, which is due to a gradual increase in the anisotropy. It indicates the gradual restricted motions of the encapsulated NR molecules on varying size. In addition, the time-resolved anisotropic investigation is also performed by varying the concentrations of encapsulated dye molecules inside PVK polymer nanoparticles (with the same size of PVK NPs) which is shown in Figure 6B. The $r(0)$ values are 0.32 and 0.17 for the 0.5 and 1.8 wt % NR-doped system, respectively. Interestingly, the average reorientation times are 3.57 and 0.545 ns for 0.5 and 1.8 wt %

Table 3. Anisotropic Decay Parameters of NR-Encapsulated PVK Nanoparticles

systems	r_0	τ_{slow} (ns) (a)	τ_{fast} (ns) ($1 - a$)	$\langle\tau_r\rangle$ (ns)
1.5 wt % NR-doped 40 nm PVK NP	0.14	2.5 (0.20)	0.44 (0.80)	0.876
1.5 wt % NR-doped 60 nm PVK NP	0.24	6.49 (0.23)	0.49 (0.77)	1.86
1.5 wt % NR-doped 100 nm PVK NP	0.27	22.10 (0.22)	0.47(0.78)	2.01
0.5 wt % NR-doped 100 nm PVK NP	0.38	15.97 (0.20)	0.47 (0.80)	3.57
1.8 wt % NR-doped 100 nm PVK NP	0.20	1.32 (0.11)	0.45 (0.84)	0.545

NR-doped PVK NP systems. It is noteworthy that the anisotropy decreases with increasing concentration of NR inside the PVK nanoparticle, indicating the energy transfer between different conformations of NR dye molecules which depolarized the emission spectra and as a result of the reduction of anisotropy is observed.[50]

Again, we evaluate the photostability of NR-encapsulated PVK nanoparticles and compare the photostability with free NR in water. Figure 7A represents the photobleaching profiles

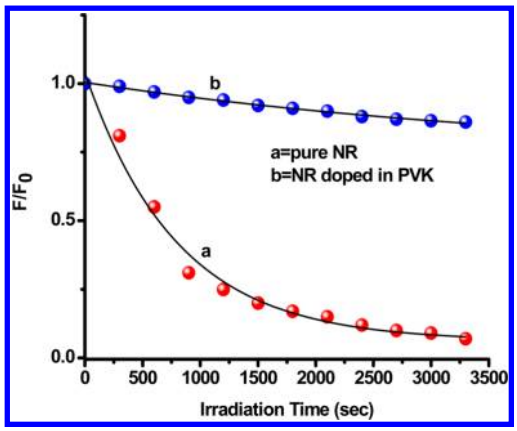

Figure 7. Temporal evolution of fluorescence intensity (photostability behavior) of free NR in aerated water (a) and NR encapsulated in PVK polymer NPs under visible light irradiation (40 W) (b).

of two consecutive systems (pure NR and NR doped in PVK nanoparticles) under equivalent conditions of photoactivation. Interestingly, NR-encompassed PVK shows ca. 15-fold enhancement in the photostability when compared with free NR molecules in water. The exceptional photostability of NR in PVK nanoparticles is attributed to the protection of dye molecules from dissolved oxygen in a freely diffusing outer sphere aqueous environment. These observations suggest that incorporation of NR in the PVK nanoparticles introduces synergistic interplay of two prerequisite factors for bioimaging: enhanced particle brightness and increased photostability.

CONCLUSIONS

Preparation of bright and photostable dye-doped polymer nanoparticles with varying size and NR composition is reported. Fundamental properties of the nanoparticles such as the diffusion dynamics, hydrodynamic diameter, and particle brightness have been investigated using fluorescence correlation spectroscopy. The improved quantum yield of encapsulated NR molecules is due to enhanced radiative decay rate. Time-resolved anisotropy nicely correlates the rotational relaxation dynamics of encapsulated NR molecules with the micro-viscosity, refractive index of the inner nanoparticle matrix, and amount of the NR population inside the nanoparticles. Analysis indicates that particle brightness depends both on the enhancement of radiative decay rate of encapsulated NR molecules and on population of the NR molecules inside the nanoparticles. Depolarized emission with increasing amount of encapsulated NR molecules suggests the possibility of energy transfer between different conformations of dopant NR molecules inside the confined polymeric nanodomain. Higher photobleaching decay rate illustrates the greater photostability of NR-doped polymer nanoparticle in solution. Modified photophysical properties of NR-encapsulated polymer nanoparticles as well as excellent photostability could make them ideal for applications such as drug delivery and specific in vivo/in vitro imaging.

ASSOCIATED CONTENT

Supporting Information

Calibration method, sample preparation, and theoretical intuition for FCS study. Figure S1 shows the UV−vis absorption spectra of free NR and NR doped in PVK NP (with varying nanoparticle size and dye concentrations). Figure S2 represents UV−vis absorption spectra, photoluminescence spectra, and PL excitation spectra of PVK in THF solution and in different sizes of nanoparticles. Figure S3 represents time-dependent PL spectra of NR encapsulated different sizes of PVK polymer nanoparticles. Figure S4 represents the autocorrelation curves of Rhodamine B in water. This material is available free of charge via the Internet at http://pubs.acs.org.

AUTHOR INFORMATION

Corresponding Authors

*E-mail: prakriti@iict.res.in (P.R.B.).

*E-mail: msap@iacs.res.in. Phone: (91)-33-2473-4971. Fax: (91)-33-2473-280 (A.P.).

Notes

The authors declare no competing financial interest.

ACKNOWLEDGMENTS

"DAE-SRC Outstanding Investigator Award" and Indo-Spain (DST) are gratefully acknowledged for financial support. S.B. thanks CSIR for awarding a fellowship. P.R.B. thanks Prof. Sudipta Maiti, Biophotonic Laboratory, Tata Institute of Fundamental Research, for his generous technical support to construct the FCS instrument, and DIT, Government of India (No. 12(4)/2007-PDD), is acknowledged for providing FCS kit.

REFERENCES

(1) Hubbell, J. A.; Chilkoti, A. Nanomaterials for Drug Delivery. *Science* **2012**, *337*, 303−305.

(2) Roming, M.; Lunsdorf, H.; Dittmar, K. E. J.; Feldmann, C. $ZrO(HPO_4)_{1-x}(FMN)_x$: Quick and Easy Synthesis of a Nanoscale Luminescent Biomarker. *Angew. Chem., Int. Ed.* **2010**, *49*, 632−637.

(3) West, J. L.; Halas, N. J. Engineered Nanomaterials for Biophotonics Applications: Improving Sensing, Imaging, and Therapeutics. *Ann. Rev. Biomed. Eng.* **2003**, *5*, 285−292.

(4) Prasad, P. N. *Introduction to Biophotonics*; John Wiley & Sons, Inc.: Hoboken, NJ, 2003; pp 203−249.

(5) Dubertret, B.; Skourides, P.; Norris, D. J.; Noireaux, V.; Brivanlou, A. H.; Libchaber, A. In Vivo Imaging of Quantum Dots Encapsulated in Phospholipid Micelles. *Science* **2002**, *298*, 1759−1762.
(6) Medintz, I. L.; Stewart, M. H.; Trammell, S. A.; Susumu, K.; Delehanty, J. B.; Mei, B. C.; Melinger, J. S.; Blanco-Canosa, J. B.; Dawson, P. E.; Mattoussi, H. Quantum-dot/Dopamine Bioconjugates Function as Redox Coupled Assemblies for in Vitro and Intracellular pH Sensing. *Nat. Mater.* **2010**, *9*, 676−684.
(7) Wang, H.; Tong, Q.; Yan, M. Antifouling Surfaces for Proteins Labeled with Dye-Doped Silica Nanoparticles. *Anal. Chem.* **2013**, *85*, 23−27.
(8) Burns, A.; Ow, H.; Wiesner, U. Fluorescent Core-Shell Silica Nanoparticles: Towards "Lab on a Particle" Architectures for Nanobiotechnology. *Chem. Soc. Rev.* **2006**, *35*, 1028−1042.
(9) Wang, F. T.; Tan, W. B.; Zhang, Y.; Fan, X.; Wang, M. Luminescent Nanomaterials for Biological Labelling. *Nanotechnology* **2005**, *17*, R1−R13.
(10) Larson, D. R.; Ow, H.; Vishwasrao, H. D.; Heikal, A. A.; Wiesner, U.; Webb, W. W. Silica Nanoparticle Architecture Determines Radiative Properties of Fluorophores. *Chem. Mater.* **2008**, *20*, 2677−2684.
(11) Ow, H.; Larson, D. R.; Srivastava, M.; Baird, B. A.; Webb, W. W.; Wiesner, U. Bright and Stable Core-Shell Fluorescent Silica Nanoparticles. *Nano Lett.* **2005**, *5*, 113−117.
(12) Roy, S.; Woolley, R.; MacCraith, B. D.; McDonagh, C. Fluorescence Lifetime Analysis and Fluorescence Correlation Spectroscopy Elucidate the Internal Architecture of Fluorescent Silica Nanoparticles. *Langmuir* **2010**, *26*, 13741−13746.
(13) Muddana, H. S.; Morgan, T. T.; Adair, J. H.; Butler, P. J. Photophysics of Cy3-Encapsulated Calcium Phosphate Nanoparticles. *Nano Lett.* **2009**, *9*, 1559−1566.
(14) Mailander, V.; Landfester, K. Interaction of Nanoparticles with Cells. *Biomacromolecules* **2009**, *10*, 2379−2400.
(15) Jin, Y.; Ye, F.; Zeigler, M.; Wu, C.; Chiu, D. T. Near-Infrared Fluorescent Dye-Doped Semiconducting Polymer Dots. *ACS Nano* **2011**, *5*, 1468−1475.
(16) Wu, W. C.; Chen, C. Y.; Tian, Y.; Jang, S. H.; Hong, Y.; Liu, Y.; Hu, R.; Tang, B. Z.; Lee, Y. T.; Chen, C. T.; et al. Enhancement of Aggregation-Induced Emission in Dye-Encapsulating Polymeric Micelles for Bioimaging. *Adv. Funct. Mater.* **2010**, *20*, 1413−1423.
(17) Wu, C.; Zheng, Y.; Szymanski, C.; McNeill, J. Energy Transfer in a Nanoscale Multichromophoric System: Fluorescent Dye-Doped Conjugated Polymer Nanoparticles. *J. Phys. Chem. C* **2008**, *112*, 1772−1781.
(18) Wu, C.; Bull, B.; Christensen, K.; McNeill, J. Ratiometric Single-Nanoparticle Oxygen Sensors for Biological Imaging. *Angew. Chem., Int. Ed.* **2009**, *48*, 2741−2745.
(19) Kumar, R.; Ohulchanskyy, T. Y.; Roy, I.; Gupta, S. K.; Borek, C.; Thomson, M. E.; Prasad, P. N. Near-Infrared Phosphorescent Polymeric Nanomicelles: Efficient Optical Probes for Tumor Imaging and Detection. *ACS Appl. Mater. Interfaces* **2009**, *1*, 1474−1481.
(20) Tuncel, D.; Demir, H. V. Conjugated Polymer Nanoparticles. *Nanoscale* **2010**, *2*, 484−494.
(21) Pecher, J.; Mecking, S. Nanoparticles of Conjugated Polymers. *Chem. Rev.* **2010**, *110*, 6260−6279.
(22) Bhattacharyya, S.; Paramanik, B.; Patra, A. Energy Transfer and Confined Motion of Dyes Trapped in Semiconducting Conjugated Polymer Nanoparticles. *J. Phys. Chem. C* **2011**, *115*, 20832−20839.
(23) Wu, C.; Chiu, D. T. Highly Fluorescent Semiconducting Polymer Dots for Biology and Medicine. *Angew. Chem., Int. Ed.* **2013**, *52*, 3086−3109.
(24) Wang, X.; Drew, C.; Lee, S. H.; Senecal, K. J.; Kumar, J.; Samuelson, L. A. Electrospun Nanofibrous Membranes for Highly Sensitive Optical Sensors. *Nano Lett.* **2002**, *2*, 1273−1275.
(25) Camposeo, A.; Benedetto, F. D.; Stabile, R.; Neves, A. A. R.; Cingolani, R.; Pisignano, D. Laser Emission from Electrospun Polymer Nanofibers. *Small* **2009**, *5*, 562−566.
(26) Fasano, V.; Polini, A.; Morello, G.; Moffa, M.; Camposeo, A.; Pisignano, D. Bright Light Emission and Wave guiding in Conjugated Polymer Nanofibers Electrospun from Organic Salt Added Solutions. *Macromolecules* **2013**, *46*, 5935−5942.
(27) Zhao, J. J.; Bae, S. C.; Xie, F.; Granick, S. Diffusion of Polymer-Coated Nanoparticles Studied by Fluorescence Correlation Spectroscopy. *Macromolecules* **2001**, *34*, 3123−3126.
(28) Schaeffel, D.; Staff, R. H.; Butt, H. J.; Landfester, K.; Crespy, D.; Koynov, K. Fluorescence Correlation Spectroscopy Directly Monitors Coalescence during Nanoparticle Preparation. *Nano Lett.* **2012**, *12*, 6012−6017.
(29) Kunst, B. H.; Schots, A.; Visser, A. J. W. G. Detection of Flowing Fluorescent Particles in a Microcapillary Using Fluorescence Correlation Spectroscopy. *Anal. Chem.* **2002**, *74*, 5350−5357.
(30) Medina, S. D.; McDonough, S.; Swanglap, P.; Landes, C. F.; Link, S. In Situ Measurement of Bovine Serum Albumin Interaction with Gold Nanospheres. *Langmuir* **2012**, *28*, 9131−9139.
(31) Neugart, F.; Zappe, A.; Jelezko, F.; Tietz, C.; Boudou, J. P.; Krueger, A.; Wrachtrup, J. Dynamics of Diamond Nanoparticles in Solution and Cells. *Nano Lett.* **2007**, *7*, 3588−3591.
(32) Rigler, P.; Meier, W. Encapsulation of Fluorescent Molecules by Functionalized Polymeric Nanocontainers: Investigation by Confocal Fluorescence Imaging and Fluorescence Correlation Spectroscopy. *J. Am. Chem. Soc.* **2006**, *128*, 367−373.
(33) Prashanthi, S.; Lanke, S. R.; Kumar, P. H.; Siva, D.; Bangal, P. R. Determination of Hydrodynamic Properties of Bare Gold and Silver Nanoparticles as a Fluorescent Probe Using its Surface-Plasmon-Induced Photoluminescence by Fluorescence Correlation Spectroscopy. *Appl. Spectrosc.* **2012**, *66*, 835−841.
(34) Weiss, S.; Pinaud, F.; Tsay, J. M.; Doose, S. Comparison of Photophysical and Colloidal Properties of Biocompatible Semiconductor Nanocrystals Using Fluorescence Correlation Spectroscopy. *Anal. Chem.* **2005**, *77*, 2235−2242.
(35) Röcker, C.; Pötzl, M.; Zhang, F.; Parak, W. J.; Nienhaus, G. U. A Quantitative Fluorescence Study of Protein Monolayer Formation on Colloidal Nanoparticles. *Nat. Nanotech.* **2009**, *4*, 577−580.
(36) Sharma, S.; Pal, N.; Chowdhury, P. K.; Sen, S.; Ganguli, A. K. Understanding Growth Kinetics of Nanorods in Microemulsion: A Combined Fluorescence Correlation Spectroscopy, Dynamic Light Scattering and Electron Microscopy Study. *J. Am. Chem. Soc.* **2012**, *134*, 19677−19684.
(37) Bhattacharyya, S.; Sen, T.; Patra, A. Host−Guest Energy Transfer: Semiconducting Polymer Nanoparticles and Au Nanoparticles. *J. Phys. Chem. C* **2010**, *114*, 11787−11795.
(38) Lakowicz, J. R. *Principles of Fluorescence Spectroscopy*, 3rd ed.; Kluwer Academic/ Plenum Publishers: New York, 1999; pp 354−464.
(39) Eigen, M.; Rigler, R. Sorting Single Molecules: Application to Diagnostics and Evolutionary Biotechnology. *Proc. Natl. Acad. Sci. U.S.A.* **1994**, *91*, 5740−5747.
(40) Thompson, N. L. *Topics in Fluorescence Spectroscopy: Techniques*; Plenum Press: New York, 1991; Vol. *1*, pp 337−378.
(41) Hess, S. T.; Huang, S.; Heikal, A. A.; Webb, W. W. Biological and Chemical Applications of Fluorescence Correlation Spectroscopy: A Review. *Biochemistry* **2002**, *41*, 697−705.
(42) Sengupta, P.; Garai, K.; Balaji, J.; Periasamy, N.; Maiti, S. Measuring Size Distribution in Highly Heterogeneous Systems with Fluorescence Correlation Spectroscopy. *Biophys. J.* **2003**, *84*, 1977−1984.
(43) Grey, J. K.; Kim, D. Y.; Norris, B. C.; Miller, W. L.; Barbara, P. F. Size-Dependent Spectroscopic Properties of Conjugated Polymer Nanoparticles. *J. Phys. Chem. B* **2006**, *110*, 25568−25572.
(44) Nguyen, T. Q.; Doan, V.; Schwartz, B. J. Conjugated Polymer Aggregates in Solution: Control of Interchain Interactions. *J. Chem. Phys.* **1999**, *110*, 4068−4078.
(45) Kurokawa, N.; Yoshikawa, H.; Hirota, N.; Hyodo, K.; Masuhara, H. Size-Dependent Spectroscopic Properties and Thermochromic Behavior in Poly(substituted thiophene) Nanoparticles. *ChemPhysChem* **2004**, *5*, 1609−1615.
(46) Mukherjee, S.; Kombrabail, M.; Krishnamoorthy, G.; Chattopadhyay, A. Dynamics and Heterogeneity of Bovine Hippo-

campal Membranes: Role of Cholesterol and Proteins. *Biochim. Biophys. Acta* **2007**, *1768*, 2130−2144.
(47) Sarkar, N.; Das, K.; Nath, D. N.; Bhattacharyya, K. Twisted Charge Transfer Processes of Nile red in Homogeneous Solutions and in Faujasite Zeolite. *Langmuir* **1994**, *10*, 326−329.
(48) Zhu, Y.; Wei, M.; Shao, Q.; Lu, L.; Lu, X.; Shen, W. Molecular Dynamics Study of Pore Inner Wall Modification Effect in Structure of Water Molecules Confined in Single-Walled Carbon Nanotubes. *J. Phys. Chem. C* **2009**, *113*, 882−889.
(49) Dutt, G. B. Rotational Diffusion of Hydrophobic Probes in Brij-35 Micelles: Effect of Temperature on Micellar Internal Environment. *J. Phys. Chem. B* **2003**, *107*, 10546−10551.
(50) Berberan-Santos, M. N.; Valeur, B. Fluorescence Depolarization by Electronic Energy Transfer in Donor-Acceptor Pairs of Like and Unlike Chromophores. *J. Chem. Phys.* **1991**, *95*, 8048−8055.